Journal of Computational Mathematics
Vol.xx, No.x, 2025, 1–16.

http://www.global-sci.org/jcm
doi:10.4208/jcm.2504-m2025-0005

A NEW COUPLED SUBDIFFUSION MODEL AND ITS PARTITIONED TIME-STEPPING ALGORITHM*

Zheng Li
School of Mathematics and Statistics, Donghua University, Shanghai 201620, China;
School of Aeronautics and Astronautics, Shanghai Jiao Tong University, Shanghai 200240, China
Email: ilizheng@msn.com

Yuting Xiang
School of Mathematical Sciences, East China Normal University, Shanghai 200241, China
Email: 52265500029@stu.ecnu.edu.cn

Hui Xu
School of Aeronautics and Astronautics, Shanghai Jiao Tong University, Shanghai 200240, China
Email: dr.hxu@sjtu.edu.cn

Jiaping Yu[1)]
School of Mathematics and Statistics, Donghua University, Shanghai 201620, China
Email: jpyu@dhu.edu.cn

Haibiao Zheng
Ministry of Education Key Laboratory of Mathematics and Engineering Applications, Shanghai Key Laboratory of PMMP, East China Normal University, Shanghai 200241, China
Email: hbzheng@math.ecnu.edu.cn

Abstract

This paper investigates an interface-coupled fractional subdiffusion model, featuring two subdiffusion equations in adjacent domains connected by an interface allowing bidirectional energy transfer. The fractional derivative, accounting for long-term medium effects, introduces challenges in theoretical analysis and computational efficiency. We propose a partitioned time-stepping algorithm using higher-order extrapolations on the interface term to decouple the system with improved temporal accuracy, combined with finite element spatial approximations. Rigorous theoretical analysis demonstrates unconditional stability and optimal L^2 norm error estimates, supported by several numerical experiments.

Mathematics subject classification: 35R11, 65M60, 65M12.
Key words: Time-fractional derivative, Interface-coupled problem, Partitioned time-stepping method, Stability, Error estimate.

1. Introduction

There are many problems in which different physical models, different parameter regimes, or different solution behaviors are coupled across interfaces, such as atmosphere-ocean coupling and fluid-solid interaction problems [1, 2, 4, 25, 32]. In recent years, significant attention has been devoted to multi-domain, multi-physics coupled problems [3, 5, 12, 13, 19]. Particularly,

* Received January 9, 2024 / Revised version received September 25, 2024 / Accepted April 3, 2025 / Published online May 8, 2025 /
1) Corresponding author.

many innovative numerical simulation methods have been developed for fluid-fluid interactions [6, 10, 15, 17, 29]. Connors *et al.* [8, 9] introduced a partitioned time-stepping method to naturally decouple multidomain multiphysics systems, using a simplified atmosphere-ocean interaction model with deterministic friction parameter κ as a linear heat-heat coupled system. They proposed fully implicit, implicit-explicit partitioned, and data-passing partitioned schemes, proving first-order time accuracy for both partitioned schemes and extending the method to nonlinear models. Given that coupled fluid-fluid and fluid-structure interaction dilemmas result in large and ill-conditioned systems of algebraic equations, partitioned techniques have frequently been employed to break down the interconnected problem into smaller, better-conditioned subproblems [9, 20, 33].

Ongoing research demands increasingly precise models to study sophisticated materials and anomalous diffusion phenomena in physics. Fractional differential operators effectively describe phenomena involving long-term or nonlocal interactions [11, 14, 23]. Consequently, there has been significant interest in developing its theory and numerical analyses for fractional differential equations [18, 30, 37, 38]. Many numerical methods have been studied for the time-fractional PDEs. Liu *et al.* [26] presented a finite difference method in both space and time for the time-fractional diffusion equation. Sun and Wu [35] considered and analyzed a finite difference scheme for the fractional diffusion wave equation. Lin and Xu [24] presented a finite difference scheme in time and Legendre spectral method in space for the time-fractional diffusion equation. Li and Yi [21] investigate an implicit-explicit scheme for 2D nonlinear time-fractional subdiffusion equation with proving the stability and convergence. Lv and Xu [28] discussed a high order finite difference method to approximate the fractional derivative in time, resulting in a time stepping scheme for the underlying equation, and analyzed the stability and convergence of the time stepping scheme. Li *et al.* [22] established a fractional Gronwall inequality for the $L1$ approximation to the Caputo fractional derivative and provided optimal error estimates for several fully discrete linearized Galerkin finite element methods for nonlinear problems. Wang and Zheng [36, 40] explore finite element and finite difference approximations of time-fractional diffusion equations, focusing on regularity properties and conducting detailed error analysis. Zhang *et al.* [39] study a weighted and shifted Grünwald-Letnikov difference Legendre spectral method for 2D nonlinear time fractional mobile/immobile advection-dispersion equation and prove its stability and convergence. Luo *et al.* [27] present a numerical scheme based on compact finite difference for solving time fractional equation with the accuracy is not dependent on the fractional order. Qi and Xu [31] examine the stochastic time-fractional heat diffusion equation with a random diffusion coefficient field and fractionally multiplicative noise, providing the problem's well-posedness and the numerical scheme's convergence.

However, multidomain coupled subdiffusion problems have received less attention. Drawing inspiration from decoupling methods for parabolic problems with dual subdomains [33, 34], we introduce a partitioned time-stepping algorithm for a linear interface-coupled subdiffusion model. We employ higher-order extrapolations on the interface term to decouple the system, requiring only information exchange across the interface at each time step. This is followed by the independent resolution of each subproblem, with both subdomain solvers operating as black boxes.

The structure of this paper is as follows. In Section 2, we present some notations and collect preliminary lemmas. Section 3 is dedicated to proving the stability of the algorithm. In Section 4, we provide an error analysis of the algorithm and Section 5 present some numerical experiments that illustrate the theoretical results.

2. Interface-coupled Subdiffusion Problem

2.1. Formulation of the coupled problem

In this section, we will consider a pair of heat transfer systems interconnected by interface conditions that enable bidirectional energy transfer across the interface. Let the domain $\Omega \subset \mathbb{R}^d$ $(d = 2, 3)$ consist of two convex, polygonal subdomains Ω_i, $i = 1, 2$ with the interface $\Gamma = \partial\Omega_1 \cap \partial\Omega_2$, the outer boundary of each subdomain $\Gamma_i = \partial\Omega_i \backslash \Gamma$, the unit outward normal vector $\hat{n}_i$ to $\partial\Omega_i$. Fig. 2.1 is a simple 2D example for the domain.

The pair of heat equations interconnected by the interface conditions are shown as follows:

$$\begin{aligned} {}_0^C D_t^\alpha u_i - \nabla \cdot (\nu_i \nabla u_i) &= f_i \quad \text{in } \Omega_i \times [0, T], \\ -\nu_i \nabla u_i \cdot \hat{n}_i &= \kappa(u_i - u_m) \quad \text{on } \Gamma \times [0, T], \\ u_i(x, 0) &= u_i^0(x) \quad \text{in } \Omega_i, \\ u_i(x, t) &= 0 \quad \text{on } \Gamma_i \end{aligned} \tag{2.1}$$

with $i, m = 1, 2$ and $i \neq m$. In this system, ν_i denotes the thermal conductivity which has a positive lower bound and $\bar{\nu}^{-1} := \max\{\nu_1^{-1}, \nu_2^{-1}\}$, $f_i(t, x)$ is the sink/source term, and $\kappa > 0$ means the friction parameter, which is calculated in practice from the bulk flux formulae [7]. The Caputo fractional derivative of a function $\omega(t)$ is defined by [11]

$${}_0^C D_t^\alpha \omega(t) = \begin{cases} \dfrac{1}{\Gamma(1-\alpha)} \displaystyle\int_0^t \frac{\omega'(s)}{(t-s)^\alpha} ds, & 0 < \alpha < 1, \\ \omega'(t), & \alpha = 1 \end{cases}$$

with $\Gamma(\cdot)$ stands for the Gamma function. Here, we will use the $L1$ approximation to discretize the Caputo derivative in the numerical scheme for (2.1). Let N be a positive integer and $\tau := T/N$ be the time step size. A temporal partition on $[0, T]$ can be defined by $t_n := n\tau$ for $n = 0, 1, \ldots, N$. Given the temporal partition, the Caputo derivative could be discretized at time $t = t_n$ as [23, 28]

$${}_0^C D_{t_n}^\alpha \omega(t) = D_\tau^\alpha \omega^n + \mathcal{O}(\tau^{2-\alpha}) \tag{2.2}$$

with

$$D_\tau^\alpha \omega^n := \frac{1}{\mu_\tau^\alpha} \sum_{j=1}^{n} a_{n-j} \delta_t \omega^j,$$

and ω^n for the numerical approximation of $\omega(t_n)$,

$$\mu_\tau^\alpha = \Gamma(2-\alpha)\tau^\alpha, \quad \delta_t \omega^j = \omega^j - \omega^{j-1}, \quad a_j = (j+1)^{1-\alpha} - j^{1-\alpha}.$$

It is clear that the coefficients form a monotonically decreasing positive sequence, $1 = a_0 > a_1 > a_2 > \cdots > 0$.

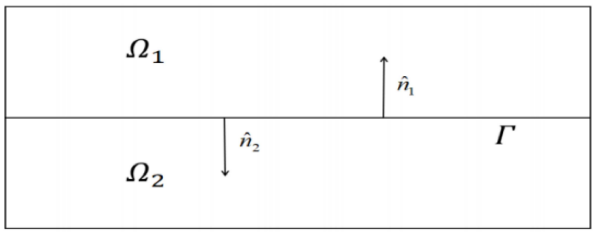

Fig. 2.1. Example for the subdomains adjoined by an interface Γ.

2.2. Weak formulation

Some notations for the Hilbert spaces are introduced first. We use $\|\cdot\|_0$ and $(\cdot\,,\cdot)$ to denote the L^2-norm and inner product on each subdomain, and $\|\cdot\|_\Gamma$ to denote the $L^2(\Gamma)$-norm on the interface. For $i = 1, 2$, let

$$X_i := \left\{v \in H^1(\Omega_i) : v = 0 \text{ on } \Gamma_i\right\}$$

be the Sobolev space for each subdomain. Actually, the seminorm $\|\nabla v\|_0$ is a norm for $v \in X_i$, so that the space X_i can be equipped with the norm $\|v\|_1 := \|\nabla v\|_0$. For the global domain, two product spaces are defined by

$$\begin{aligned} &X = X_1 \times X_2 = \{\mathbf{v} = (v_1, v_2) : v_i \in X_i,\ i = 1, 2\},\\ &L^2(\Omega) = L^2(\Omega_1) \times L^2(\Omega_2), \end{aligned}$$

and they are equipped with the following norms for $\mathbf{u} \in L^2(\Omega)$ and $\mathbf{v} \in X$:

$$\|\mathbf{u}\|_0^2 = \sum_{i=1}^{2} \|u_i\|_0^2, \quad \|\mathbf{v}\|_1^2 = \sum_{i=1}^{2} \|v_i\|_1^2.$$

And the notation for $L^2(\Gamma)$-norm, $\|\cdot\|_\Gamma$, can also be used as

$$\|\mathbf{u}\|_\Gamma^2 = \sum_{i=1}^{2} \|u_i\|_\Gamma^2.$$

Moreover, we define two weighted norms as

$$\|\mathbf{u}\|_{0,\nu}^2 = \sum_{i=1}^{2} \frac{\|u_i\|_0^2}{\nu_i}, \quad \|\mathbf{v}\|_{1,\nu}^2 = \sum_{i=1}^{2} \nu_i \|v_i\|_1^2.$$

If we define the bilinear form $a : X \times X \to \mathbb{R}$ in the following way, for $\mathbf{u} = (u_1, u_2)$ and $\mathbf{v} = (v_1, v_2) \in X$,

$$a(\mathbf{u}, \mathbf{v}) = (\nu \nabla \mathbf{u}, \nabla \mathbf{v}) + \int_\Gamma \kappa [\mathbf{u}][\mathbf{v}] \mathrm{d}s, \tag{2.3}$$

where $[\cdot]$ denotes the jump of the indicated quantity across the interface, then the weak formulation for the fractional interface-coupled subdiffusion problem is as follows: Seek $\mathbf{u} = (u_1, u_2) \in X$ such that

$$\left({}_0^C D_t^\alpha \mathbf{u}, \mathbf{v}\right) + a(\mathbf{u}, \mathbf{v}) = (\mathbf{f}, \mathbf{v}), \quad \forall\, \mathbf{v} \in X. \tag{2.4}$$

In order to construct the numerical scheme for the problem, we consider a regular, quasi-uniform triangulation ($d = 2$) or tetrahedron ($d = 3$) $\mathcal{T}_i$ for each subdomain Ω_i, with $\mathcal{T}_1$ and $\mathcal{T}_2$ compatible at the interface Γ. And $\mathcal{T}_h := \mathcal{T}_1 \cup \mathcal{T}_2$ with mesh size h is defined for the global domain Ω. For $i = 1, 2$, let $X_{i,h} \subset X_i$ be the finite element spaces and satisfy $X_h = X_{1,h} \times X_{2,h} \subset X$. Furthermore, we recall the Poincaré inequality and trace inequality as follows. There exist strictly positive constants C_p and C_t only depending on the domain Ω such that for $\mathbf{v} \in X_h$,

$$\|\mathbf{v}\|_0 \le C_p \|\mathbf{v}\|_1, \quad \|\mathbf{v}\|_\Gamma^2 \le C_t \|\mathbf{v}\|_0 \|\mathbf{v}\|_1.$$

Based on the weak form (2.4) and the discretization of the Caputo derivative, a fully, monolithically coupled implicit scheme is proposed as follows.

Algorithm 2.1: Coupled Scheme.

Given $\mathbf{u}_h^0 \in X_h$, find $\mathbf{u}_h^n \in X_h$ such that

$$\big(D_\tau^\alpha \mathbf{u}_h^n, \mathbf{v}\big) + a\big(\mathbf{u}_h^n, \mathbf{v}\big) = (\mathbf{f}^n, \mathbf{v}), \quad \forall\, \mathbf{v} \in X_h \tag{2.5}$$

for $n = 1, 2, \ldots, N$, where $\mathbf{f}^n := \mathbf{f}(t_n)$.

The main purpose of this paper is to present a partitioned time-stepping algorithm for the interface-coupled subdiffusion problem, which requires only to solve one, uncoupled subdiffusion subproblem in each subdomain per time step.

3. Partitioned Time-stepping Algorithm and Its Stability

The partitioned time-stepping algorithm for the coupled model (2.1) is presented in this section, along with an analysis of its unconditional stability. To decouple the problem and preserve the accuracy of (2.2), we utilize second-order extrapolations in the interface integral terms.

Algorithm 3.1: Partitioned Time-stepping Algorithm.

Given $\mathbf{u}_h^0 \in X_h$, get $\mathbf{u}_h^1$ from the coupled scheme Algorithm 2.1. For $n \geq 2$, solve the equations for $u_{1,h}^n$ and $u_{2,h}^n$ according to the following Subproblem 1 and Subproblem 2, respectively.

Subproblem 1. In Ω_1, find $u_{1,h}^n \in X_{1,h}$ satisfies that for any $v_1 \in X_{1,h}$,

$$\big(D_\tau^\alpha u_{1,h}^n, v_1\big) + \big(\nu_1 \nabla u_{1,h}^n, \nabla v_1\big) + \int_\Gamma \kappa\big(u_{1,h}^n - 2u_{2,h}^{n-1} + u_{2,h}^{n-2}\big) v_1 \mathrm{d}s = \big(f_1^n, v_1\big). \tag{3.1}$$

Subproblem 2. In Ω_2, find $u_{2,h}^n \in X_{2,h}$ satisfies that for any $v_2 \in X_{2,h}$,

$$\big(D_\tau^\alpha u_{2,h}^n, v_2\big) + \big(\nu_2 \nabla u_{2,h}^n, \nabla v_2\big) + \int_\Gamma \kappa\big(u_{2,h}^n - 2u_{1,h}^{n-1} + u_{1,h}^{n-2}\big) v_2 \mathrm{d}s = \big(f_2^n, v_2\big). \tag{3.2}$$

Here, we use different schemes for $\mathbf{u}_h^1$ and $\mathbf{u}_h^n$ ($n \geq 2$). So two different theorems are presented to show the stability.

Theorem 3.1. *Suppose that* $\mathbf{f}^1 \in L^2(0, T; L^2(\Omega))$ *and* $\mathbf{u}_h^1 \in X_h$ *satisfy* (2.5). *Then we have*

$$\big\|\mathbf{u}_h^1\big\|_0^2 + \mu_\tau^\alpha \big\|\mathbf{u}_h^1\big\|_{1,\nu}^2 \leq \big\|\mathbf{u}_h^0\big\|_0^2 + \frac{t_1^\alpha C_p^2}{\Gamma(1+\alpha)} \|\mathbf{f}^1\|_{0,\nu}^2. \tag{3.3}$$

Proof. Taking $\mathbf{v} = 2\mathbf{u}_h^1$ in (2.5), we have

$$2\big(D_\tau^\alpha \mathbf{u}_h^1, \mathbf{u}_h^1\big) + 2\big(\nu \nabla \mathbf{u}_h^1, \nabla \mathbf{u}_h^1\big) + 2\kappa \big\|\mathbf{u}_h^1\big\|_\Gamma^2 = 2\big(\mathbf{f}^1, \mathbf{u}_h^1\big) + 4\kappa \int_\Gamma u_{1,h}^1 u_{2,h}^1 \mathrm{d}s. \tag{3.4}$$

For the second term on the right-hand side of (3.4), using Cauchy-Schwarz inequality and Young's inequality, we have

$$4\kappa \int_\Gamma u_{1,h}^1 u_{2,h}^1 \mathrm{d}s \leq 4\kappa \big\|u_{1,h}^1\big\|_\Gamma \big\|u_{2,h}^1\big\|_\Gamma \leq 2\kappa \big\|\mathbf{u}_h^1\big\|_\Gamma^2, \tag{3.5}$$

which will eliminate the same term on the left-hand side. Employing the same inequalities for the first term on the right-hand side of (3.4), we get the following with Poincaré inequality:

$$2\big(\mathbf{f}^1, \mathbf{u}_h^1\big) \le C_p^2 \|\mathbf{f}^1\|_{0,\nu}^2 + \big\|\mathbf{u}_h^1\big\|_{1,\nu}^2. \tag{3.6}$$

Together with the property of $L1$ discretization of the Caputo derivative (see [22])

$$2\big(D_\tau^\alpha \mathbf{u}_h^1, \mathbf{u}_h^1\big) \ge D_\tau^\alpha \big\|\mathbf{u}_h^1\big\|_0^2,$$

we can obtain

$$D_\tau^\alpha \big\|\mathbf{u}_h^1\big\|_0^2 + \big\|\mathbf{u}_h^1\big\|_{1,\nu}^2 \le C_p^2 \|\mathbf{f}^1\|_{0,\nu}^2. \tag{3.7}$$

Multiplying (3.7) by $\mu_\tau^\alpha = \Gamma(2-\alpha)\tau^\alpha$, we conclude

$$\big\|\mathbf{u}_h^1\big\|_0^2 + \mu_\tau^\alpha \big\|\mathbf{u}_h^1\big\|_{1,\nu}^2 \le \big\|\mathbf{u}_h^0\big\|_0^2 + \mu_\tau^\alpha C_p^2 \|\mathbf{f}^1\|_{0,\nu}^2. \tag{3.8}$$

And this completes the proof with $\Gamma(2-\alpha) \le 1/(\Gamma(1+\alpha))$ for $0 < \alpha \le 1$ and $t_1 = \tau$. □

To overcome the difficulties due to the long time interactions of fractional derivatives, a sequence $\{p_n\}$ is introduced [22],

$$p_0 = 1, \quad p_n = \sum_{j=1}^{n} (a_{j-1} - a_j) p_{n-j}, \quad n \ge 1. \tag{3.9}$$

It is easy to verify inductively that $0 < p_n < 1$ $(n \ge 1)$. Additionally, it possesses three important properties that are useful in the following proofs:

$$p_{n+1} \ge (2 - 2^{1-\alpha}) p_n, \qquad n \ge 0, \tag{3.10}$$

$$\sum_{j=k}^{n} p_{n-j} a_{j-k} = 1, \qquad 1 \le k \le n, \tag{3.11}$$

$$\Gamma(2-\alpha) \sum_{j=1}^{n} p_{n-j} \le \frac{n^\alpha}{\Gamma(1+\alpha)}. \tag{3.12}$$

Theorem 3.2. *Suppose that* $\mathbf{f}^n \in L^2(0,T;L^2(\Omega))$ *for* $n = 1, 2, \ldots, N$ *and* $\{\mathbf{u}_h^n\}_{n=2}^N$ *are obtained by Algorithm* 3.1*, then there exists a positive constant* λ *such that*

$$\big\|\mathbf{u}_h^n\big\|_0^2 + \mu_\tau^\alpha \big\|\mathbf{u}_h^n\big\|_{1,\nu}^2 \le \Psi_{1n} E_\alpha\big(2\lambda t_n^\alpha\big) \tag{3.13}$$

with

$$\Psi_{1n} := \left(1 + \frac{C_t^2 \kappa^2 \mu_\tau^\alpha}{2(2-2^{1-\alpha})^2 \bar{\nu}}\right) \big\|\mathbf{u}_h^0\big\|_0^2 + \mu_\tau^\alpha \big\|\mathbf{u}_h^0\big\|_{1,\nu}^2 + \frac{t_n^\alpha C_p^2}{\Gamma(1+\alpha)} \max_{1\le j\le n} \|\mathbf{f}^j\|_{0,\nu}^2,$$

$$\lambda = \frac{4C_t^2\kappa^2}{(2-2^{1-\alpha})^2\bar{\nu}} + \frac{C_t^2\kappa^2}{4(2-2^{1-\alpha})^4\bar{\nu}},$$

and the Mittag-Leffler function

$$E_\alpha(z) = \sum_{k=0}^{\infty} \frac{z^k}{\Gamma(1+k\alpha)}.$$

Proof. For $j \geq 2$, taking $v_1 = 2u_{1,h}^j$ in (3.1), we have

$$\begin{aligned} &2\big(D_\tau^\alpha u_{1,h}^j, u_{1,h}^j\big) + 2\nu_1\big\|u_{1,h}^j\big\|_1^2 + 2\kappa\big\|u_{1,h}^j\big\|_\Gamma^2 \\ &= 2\big(f_1^j, u_{1,h}^j\big) + 2\kappa\int_\Gamma \big(2u_{2,h}^{j-1} - u_{2,h}^{j-2}\big)u_{1,h}^j \mathrm{d}s. \end{aligned} \tag{3.14}$$

For the first term on the right-hand side, similar to the procedures in the Theorem 3.1, we have

$$2\big(f_1^j, u_{1,h}^j\big) \leq \frac{C_p^2}{\nu_1}\big\|f_1^j\big\|_0^2 + \nu_1\big\|u_{1,h}^j\big\|_1^2. \tag{3.15}$$

As the second term on the right-hand side, utilizing Cauchy-Schwarz inequality, Young's inequality, Minkowski inequality and trace inequality, we can obtain that

$$\begin{aligned} &2\kappa\int_\Gamma \big(2u_{2,h}^{j-1} - u_{2,h}^{j-2}\big)u_{1,h}^j \mathrm{d}s \\ &\leq \frac{\kappa}{2}\big\|2u_{2,h}^{j-1} - u_{2,h}^{j-2}\big\|_\Gamma^2 + 2\kappa\big\|u_{1,h}^j\big\|_\Gamma^2 \\ &\leq 4\kappa\big\|u_{2,h}^{j-1}\big\|_\Gamma^2 + \kappa\big\|u_{2,h}^{j-2}\big\|_\Gamma^2 + 2\kappa\big\|u_{1,h}^j\big\|_\Gamma^2 \\ &\leq \frac{\nu_2 p_{n-(j-1)}}{2p_{n-j}}\big\|u_{2,h}^{j-1}\big\|_1^2 + \frac{8C_t^2\kappa^2 p_{n-j}}{\nu_2 p_{n-(j-1)}}\big\|u_{2,h}^{j-1}\big\|_0^2 \\ &\quad + \frac{\nu_2 p_{n-(j-2)}}{2p_{n-j}}\big\|u_{2,h}^{j-2}\big\|_1^2 + \frac{C_t^2\kappa^2 p_{n-j}}{2\nu_2 p_{n-(j-2)}}\big\|u_{2,h}^{j-2}\big\|_0^2 + 2\kappa\big\|u_{1,h}^j\big\|_\Gamma^2. \end{aligned} \tag{3.16}$$

Then, we have

$$\begin{aligned} &D_\tau^\alpha\big\|u_{1,h}^j\big\|_0^2 + \nu_1\big\|u_{1,h}^j\big\|_1^2 - \frac{\nu_2 p_{n-(j-1)}}{2p_{n-j}}\big\|u_{2,h}^{j-1}\big\|_1^2 - \frac{\nu_2 p_{n-(j-2)}}{2p_{n-j}}\big\|u_{2,h}^{j-2}\big\|_1^2 \\ &\leq \frac{C_p^2}{\nu_1}\big\|f_1^j\big\|_0^2 + \frac{8C_t^2\kappa^2 p_{n-j}}{\nu_2 p_{n-(j-1)}}\big\|u_{2,h}^{j-1}\big\|_0^2 + \frac{C_t^2\kappa^2 p_{n-j}}{2\nu_2 p_{n-(j-2)}}\big\|u_{2,h}^{j-2}\big\|_0^2. \end{aligned} \tag{3.17}$$

Given $n \geq 2$, multiplying (3.17) by $\mu_\tau^\alpha p_{n-j}$ and summing over for j from 2 to n, utilizing (3.11), the first term can be rewritten as

$$\begin{aligned} &\mu_\tau^\alpha\sum_{j=2}^n p_{n-j}D_\tau^\alpha\big\|u_{1,h}^j\big\|_0^2 = \sum_{j=2}^n p_{n-j}\sum_{k=1}^j a_{j-k}\delta_t\big\|u_{1,h}^k\big\|_0^2 \\ &= \sum_{j=2}^n p_{n-j}\sum_{k=2}^j a_{j-k}\delta_t\big\|u_{1,h}^k\big\|_0^2 + \delta_t\big\|u_{1,h}^1\big\|_0^2\sum_{j=2}^n p_{n-j}a_{j-1} \\ &= \sum_{k=2}^n \delta_t\big\|u_{1,h}^k\big\|_0^2\sum_{j=k}^n p_{n-j}a_{j-k} + (1-p_{n-1})\delta_t\big\|u_{1,h}^1\big\|_0^2 \\ &= \big\|u_{1,h}^n\big\|_0^2 - p_{n-1}\big\|u_{1,h}^1\big\|_0^2 - (1-p_{n-1})\big\|u_{1,h}^0\big\|_0^2. \end{aligned} \tag{3.18}$$

Then (3.17) can be reformulated as

$$\begin{aligned} &\big\|u_{1,h}^n\big\|_0^2 + \mu_\tau^\alpha\sum_{j=2}^n\left(\nu_1 p_{n-j}\big\|u_{1,h}^j\big\|_1^2 - \frac{\nu_2 p_{n-(j-1)}}{2}\big\|u_{2,h}^{j-1}\big\|_1^2 - \frac{\nu_2 p_{n-(j-2)}}{2}\big\|u_{2,h}^{j-2}\big\|_1^2\right) \\ &\leq \mu_\tau^\alpha\sum_{j=2}^n\left(\frac{C_p^2 p_{n-j}}{\nu_1}\big\|f_1^j\big\|_0^2 + \frac{8C_t^2\kappa^2 p_{n-j}^2}{\nu_2 p_{n-(j-1)}}\big\|u_{2,h}^{j-1}\big\|_0^2 + \frac{C_t^2\kappa^2 p_{n-j}^2}{2\nu_2 p_{n-(j-2)}}\big\|u_{2,h}^{j-2}\big\|_0^2\right) \\ &\quad + p_{n-1}\big\|u_{1,h}^1\big\|_0^2 + (1-p_{n-1})\big\|u_{1,h}^0\big\|_0^2. \end{aligned} \tag{3.19}$$

Employing this similar process to (3.2), we can derive that

$$\begin{aligned}
&\big\|u_{2,h}^n\big\|_0^2+\mu_\tau^\alpha\sum_{j=2}^{n}\left(\nu_2 p_{n-j}\big\|u_{2,h}^j\big\|_1^2-\frac{\nu_1 p_{n-(j-1)}}{2}\big\|u_{1,h}^{j-1}\big\|_1^2-\frac{\nu_1 p_{n-(j-2)}}{2}\big\|u_{1,h}^{j-2}\big\|_1^2\right)\\
&\le\mu_\tau^\alpha\sum_{j=2}^{n}\left(\frac{C_p^2 p_{n-j}}{\nu_2}\big\|f_2^j\big\|_0^2+\frac{8C_t^2\kappa^2p_{n-j}^2}{\nu_1 p_{n-(j-1)}}\big\|u_{1,h}^{j-1}\big\|_0^2+\frac{C_t^2\kappa^2p_{n-j}^2}{2\nu_1 p_{n-(j-2)}}\big\|u_{1,h}^{j-2}\big\|_0^2\right)\\
&\quad+p_{n-1}\big\|u_{2,h}^1\big\|_0^2+(1-p_{n-1})\big\|u_{2,h}^0\big\|_0^2.
\end{aligned}\tag{3.20}$$

Then adding together and collecting like terms, it yields that

$$\begin{aligned}
&\big\|\mathbf{u}_h^n\big\|_0^2+\mu_\tau^\alpha\big\|\mathbf{u}_h^n\big\|_{1,\nu}^2+\frac{\mu_\tau^\alpha p_1}{2}\big\|\mathbf{u}_h^{n-1}\big\|_{1,\nu}^2\\
&\le\mu_\tau^\alpha\sum_{j=2}^{n}\left(C_p^2p_{n-j}\|\mathbf{f}^j\|_{0,\nu}^2+\frac{8C_t^2\kappa^2p_{n-j}^2}{\bar\nu p_{n-(j-1)}}\big\|\mathbf{u}_h^{j-1}\big\|_0^2+\frac{C_t^2\kappa^2p_{n-j}^2}{2\bar\nu p_{n-(j-2)}}\big\|\mathbf{u}_h^{j-2}\big\|_0^2\right)\\
&\quad+p_{n-1}\big(\big\|\mathbf{u}_h^1\big\|_0^2+\mu_\tau^\alpha\big\|\mathbf{u}_h^1\big\|_{1,\nu}^2\big)+(1-p_{n-1})\big\|\mathbf{u}_h^0\big\|_0^2+\frac{\mu_\tau^\alpha p_n}{2}\big\|\mathbf{u}_h^0\big\|_{1,\nu}^2.
\end{aligned}\tag{3.21}$$

By the result (3.8) in Theorem 3.1, the properties (3.10) and (3.12), we can derive that

$$\begin{aligned}
&\big\|\mathbf{u}_h^n\big\|_0^2+\mu_\tau^\alpha\big\|\mathbf{u}_h^n\big\|_{1,\nu}^2\\
&\le\frac{8C_t^2\kappa^2\mu_\tau^\alpha}{(2-2^{1-\alpha})\bar\nu}\sum_{j=2}^{n}p_{n-j}\big\|\mathbf{u}_h^{j-1}\big\|_0^2+\frac{C_t^2\kappa^2\mu_\tau^\alpha}{2(2-2^{1-\alpha})^2\bar\nu}\sum_{j=2}^{n}p_{n-j}\big\|\mathbf{u}_h^{j-2}\big\|_0^2\\
&\quad+\big\|\mathbf{u}_h^0\big\|_0^2+\frac{\mu_\tau^\alpha p_n}{2}\big\|\mathbf{u}_h^0\big\|_{1,\nu}^2+\frac{t_n^\alpha C_p^2}{\Gamma(1+\alpha)}\max_{1\le j\le n}\|\mathbf{f}^j\|_{0,\nu}^2.
\end{aligned}\tag{3.22}$$

Let

$$\Psi_{1n}:=\left(1+\frac{C_t^2\kappa^2\mu_\tau^\alpha}{2(2-2^{1-\alpha})^2\bar\nu}\right)\big\|\mathbf{u}_h^0\big\|_0^2+\mu_\tau^\alpha\big\|\mathbf{u}_h^0\big\|_{1,\nu}^2+\frac{t_n^\alpha C_p^2}{\Gamma(1+\alpha)}\max_{1\le j\le n}\|\mathbf{f}^j\|_{0,\nu}^2$$

and we have for $1\le k\le n$, $\Psi_{1k}\le\Psi_{1n}$. With a vector defined as

$$V:=\big(\big\|\mathbf{u}_h^n\big\|_0^2+\mu_\tau^\alpha\big\|\mathbf{u}_h^n\big\|_{1,\nu}^2,\dots,\big\|\mathbf{u}_h^2\big\|_0^2+\mu_\tau^\alpha\big\|\mathbf{u}_h^2\big\|_{1,\nu}^2,\big\|\mathbf{u}_h^1\big\|_0^2+\mu_\tau^\alpha\big\|\mathbf{u}_h^1\big\|_{1,\nu}^2\big)^\top,$$

and $\vec{e}:=(1,1,\dots,1)^\top\in\mathbb{R}^n$, (3.22) can be restated in a vector form by

$$V\le\left(\frac{4C_t^2\kappa^2}{(2-2^{1-\alpha})\bar\nu}J_1+\frac{C_t^2\kappa^2}{4(2-2^{1-\alpha})^2\bar\nu}J_2\right)V+\Psi_{1n}\vec{e},\tag{3.23}$$

where two strictly upper triangular matrices $J_1,J_2\in\mathbb{R}^{n\times n}$ are given by

$$J_1=2\mu_\tau^\alpha\begin{bmatrix}0&p_0&p_1&\cdots&p_{n-2}\\0&0&p_0&\cdots&p_{n-3}\\0&0&0&\cdots&p_{n-4}\\\vdots&\vdots&\vdots&\ddots&\vdots\\0&0&0&\cdots&0\end{bmatrix},\quad J_2=2\mu_\tau^\alpha\begin{bmatrix}0&0&p_0&\cdots&p_{n-3}\\0&0&0&\cdots&p_{n-4}\\0&0&0&\cdots&p_{n-5}\\\vdots&\vdots&\vdots&\ddots&\vdots\\0&0&0&\cdots&0\end{bmatrix}.$$

Noticing that $1\ge p_n>0$ $(n\ge0)$ and using (3.10), it is trivial that

$$J_1V\le\frac{1}{\lambda(2-2^{1-\alpha})}JV,\quad J_2V\le\frac{1}{\lambda(2-2^{1-\alpha})^2}JV,\tag{3.24}$$

where

$$\lambda = \frac{4C_t^2\kappa^2}{(2-2^{1-\alpha})^2\bar{\nu}} + \frac{C_t^2\kappa^2}{4(2-2^{1-\alpha})^4\bar{\nu}},$$

and $J \in \mathbb{R}^{n\times n}$ is given by

$$J = 2\lambda\mu_\tau^\alpha \begin{bmatrix} 0 & p_1 & \cdots & p_{n-1} & p_n \\ 0 & 0 & \cdots & p_{n-2} & p_{n-1} \\ \vdots & \vdots & \ddots & \vdots & \vdots \\ 0 & 0 & \cdots & 0 & p_1 \\ 0 & 0 & \cdots & 0 & 0 \end{bmatrix}.$$

Thus, as a result of (3.23) that

$$V \le JV + \Psi_{1n}\vec{e} \le \cdots \le J^nV + \Psi_{1n}\sum_{k=0}^{n-1} J^k\vec{e}. \tag{3.25}$$

According to the properties of the strictly upper triangular matrix J in [22, Lemma 3.3], $J^n = 0$, and

$$\sum_{k=0}^{n-1} J^k\vec{e} \le \big(E_\alpha(2\lambda t_n^\alpha), \ldots, E_\alpha(2\lambda t_1^\alpha)\big)^\top,$$

(3.13) holds, which completes the proof of Theorem 3.2. □

4. Error Estimates

This section presents a convergence analysis of the method. The following two theorems demonstrate that the algorithm maintains the accuracy of (2.2) in time while achieving optimal-order convergence rates in the L^2 norm for the finite element approximations.

First of all, the solution $\mathbf{u}(t) = (u_1(t), u_2(t))$ of (2.4) is assumed to satisfy the following assumptions:

$$\mathbf{u}_t(t) \in L^2(0,T;X), \quad \mathbf{u}_{tt}(t) \in L^2\big(0,T;L^2(\Omega)\big) \cap L^\infty(0,T;X). \tag{4.1}$$

Let us define a projection operator $P_h : \mathbf{u}(t) \in X \to P_h\mathbf{u}(t) \in X_h$ (for any $t \in [0,T]$) by

$$a\big(P_h\mathbf{u}(t), \mathbf{v}\big) = a\big(\mathbf{u}(t), \mathbf{v}\big). \tag{4.2}$$

Note that P_h is a linear operator, and if $\mathbf{u}(t) \in X \cap H^{r+1}(\Omega)$, the following approximation holds:

$$\|P_h\mathbf{u}(t) - \mathbf{u}(t)\|_0 \le Ch^{r+1}\|\mathbf{u}(t)\|_{H^{r+1}(\Omega)}. \tag{4.3}$$

To estimate the error, we split the error function $\mathbf{e}^n = \mathbf{u}(t_n) - \mathbf{u}_h^n$ $(n \ge 1)$ into two parts. For simplification, we denote $P_h\mathbf{u}(t)$ by $\bar{\mathbf{u}}$ and $P_h\mathbf{u}(t_n)$ by $\bar{\mathbf{u}}^n$ for special time t_n. Then we have

$$\mathbf{e}^n = \big(\mathbf{u}(t_n) - \bar{\mathbf{u}}^n\big) + \big(\bar{\mathbf{u}}^n - \mathbf{u}_h^n\big) =: \boldsymbol{\varepsilon}^n + \boldsymbol{\delta}^n. \tag{4.4}$$

The first term of the right-hand side, $\boldsymbol{\varepsilon}^n$, can be estimated easily from (4.3) with the time taken at $t = t_n$.

Theorem 4.1. *Let* $\mathbf{u}(t)$ *and* $\mathbf{u}_h^1$ *be the solutions of* (2.4) *and* (2.5)*, respectively. Under the assumptions* (4.1)*, there is a positive constant* C *independent of* τ *or* h *such that*

$$\|\mathbf{e}^1\|_0 \leq C(\tau^{2-\alpha} + h^{r+1}). \tag{4.5}$$

Proof. First, subtracting (2.5) from (2.4), and noticing the projection (4.2) and the definition of $\boldsymbol{\delta}^1$, we have that for $t = t_1$,

$$\left(D_\tau^\alpha \boldsymbol{\delta}^1, \mathbf{v}\right) + a(\boldsymbol{\delta}^1, \mathbf{v}) = (\mathcal{R}^1, \mathbf{v}), \quad \forall\, \mathbf{v} \in X_h, \tag{4.6}$$

where

$$\mathcal{R}^1 = D_\tau^\alpha \bar{\mathbf{u}}^1 - {}_0^C D_{t_1}^\alpha \mathbf{u}(t).$$

According to the Theorem 3.1 and noting that $\boldsymbol{\delta}^0 = \bar{\mathbf{u}}^0 - \mathbf{u}_h^0 = (0, 0)$, we have that

$$\|\boldsymbol{\delta}^1\|_0^2 \leq \frac{t_1^\alpha C_p^2}{\Gamma(1+\alpha)\bar{\nu}} \|\mathcal{R}^1\|_0^2. \tag{4.7}$$

Utilizing Minkowski inequality, it follows that

$$\|\mathcal{R}^1\|_0 \leq \left\|D_\tau^\alpha \bar{\mathbf{u}}^1 - {}_0^C D_{t_1}^\alpha \bar{\mathbf{u}}\right\|_0 + \left\|{}_0^C D_{t_1}^\alpha \bar{\mathbf{u}} - {}_0^C D_{t_1}^\alpha \mathbf{u}(t)\right\|_0. \tag{4.8}$$

According the $L1$ discretization scheme (2.2) and the estimate for the projection (4.3), we have that $\|\mathcal{R}^1\|_0 \leq C(\tau^{2-\alpha} + h^{r+1})$ with a positive constant C independent of τ or h. Furthermore, by the split of error (4.4), we have that

$$\|\mathbf{e}^1\|_0 \leq \|\boldsymbol{\varepsilon}^1\|_0 + \|\boldsymbol{\delta}^1\|_0, \tag{4.9}$$

which completes the proof with (4.3) taken $t = t_1$ for estimating $\|\boldsymbol{\varepsilon}^1\|_0$. □

For $n \geq 2, \mathbf{u}_h^n$ is solved by a decoupled scheme, Algorithm 3.1, which uses second-order extrapolations in the interface integral terms. So the following estimate is critical:

$$\begin{aligned} &\|\bar{\mathbf{u}}^n - 2\bar{\mathbf{u}}^{n-1} + \bar{\mathbf{u}}^{n-2}\|_1 \\ &\leq C\|\mathbf{u}(t_n) - 2\mathbf{u}(t_{n-1}) + \mathbf{u}(t_{n-2})\|_1 \\ &\leq C\tau^2 \max_{t_{n-2} \leq t \leq t_n} \|\mathbf{u}_{tt}\|_1. \end{aligned} \tag{4.10}$$

Theorem 4.2. *Let* $\mathbf{u}(t)$ *be the solution of* (2.4) *and* $\mathbf{u}_h^n$ $(n \geq 2)$ *be solved by Algorithm* 3.1*. Under the assumptions* (4.1)*, there is a positive constant* C *independent of* τ *or* h *such that*

$$\|\mathbf{e}^n\|_0 \leq C(\tau^{2-\alpha} + h^{r+1}). \tag{4.11}$$

Proof. For $j \geq 2$, according to the definition of $\delta_1^j = \bar{u}_1^j - u_{1,h}^j$, the decoupled scheme (3.1) and the projection (4.2), we have that for any $v_1 \in X_{1,h}$,

$$\begin{aligned} &\left(D_\tau^\alpha \delta_1^j, v_1\right) + \left(\nu_1 \nabla \delta_1^j, \nabla v_1\right) + \kappa \int_\Gamma \left(\delta_1^j - 2\delta_2^{j-1} + \delta_2^{j-2}\right) v_1 \mathrm{d}s \\ &= \left(\mathcal{R}_1^j, v_1\right) + \kappa \int_\Gamma \left(\bar{u}_2^j - 2\bar{u}_2^{j-1} + \bar{u}_2^{j-2}\right) v_1 \mathrm{d}s. \end{aligned} \tag{4.12}$$

where

$$\mathcal{R}_1^j = D_\tau^\alpha \bar{u}_1^j - {}_0^C D_{t_j}^\alpha u_1(t).$$

For the right-hand side, according to the Cauchy-Schwarz inequality, Young's inequality, trace inequality and Poincaré inequality, we can get

$$\begin{aligned}
&\big(\mathcal{R}_1^j, v_1\big) + \kappa \int_\Gamma \big(\bar{u}_2^j - 2\bar{u}_2^{j-1} + \bar{u}_2^{j-2}\big) v_1 \mathrm{d}s \\
&\le \frac{2C_p^2}{\nu_1}\big\|\mathcal{R}_1^j\big\|_0^2 + \frac{\nu_1}{8}\|v_1\|_1^2 + \kappa\big\|\bar{u}_2^j - 2\bar{u}_2^{j-1} + \bar{u}_2^{j-2}\big\|_\Gamma \|v_1\|_\Gamma \\
&\le \frac{2C_p^2}{\nu_1}\big\|\mathcal{R}_1^j\big\|_0^2 + \frac{2\kappa^2 C_t^2 C_p^2}{\nu_1}\big\|\bar{u}_2^j - 2\bar{u}_2^{j-1} + \bar{u}_2^{j-2}\big\|_1^2 + \frac{\nu_1}{4}\|v_1\|_1^2. \qquad (4.13)
\end{aligned}$$

Taking $v_1 = 2\delta_1^j$, the same procedures with Theorem 3.2 can be used here. Therefore, we have that

$$\|\boldsymbol{\delta}^n\|_0^2 \le \Psi_{2n} E_\alpha\big(2\lambda t_n^\alpha\big), \qquad (4.14)$$

where

$$\Psi_{2n} = \frac{2t_n^\alpha C_p^2}{\Gamma(1+\alpha)\bar{\nu}} \max_{1\le j\le n} \|\mathcal{R}^j\|_0^2 + \frac{2t_n^\alpha \kappa^2 C_t^2 C_p^2}{\Gamma(1+\alpha)\bar{\nu}} \max_{2\le j\le n} \|\bar{\mathbf{u}}^j - 2\bar{\mathbf{u}}^{j-1} + \bar{\mathbf{u}}^{j-2}\|_1^2.$$

Similar to (4.8), $\|\mathcal{R}^j\|_0 \le C(\tau^{2-\alpha} + h^{r+1})$. Together with (4.10), we know that $\Psi_{2n} \le C(\tau^{2-\alpha} + h^{r+1})^2$. Therefore, the following estimate holds, $\|\boldsymbol{\delta}^n\|_0 \le C(\tau^{2-\alpha} + h^{r+1})$ with the coefficient depends on t_n but not on τ or h. Using Minkowski inequality, we know that

$$\|\mathbf{e}^n\|_0 \le \|\boldsymbol{\varepsilon}^n\|_0 + \|\boldsymbol{\delta}^n\|_0. \qquad (4.15)$$

Taking $t = t_n$ in (4.3) yields that $\|\boldsymbol{\varepsilon}^n\|_0 \le Ch^{r+1}$ which completes the proof with the estimate for $\boldsymbol{\delta}^n$. □

5. Numerical Experiments

In this section, we present two numerical examples to validate the accuracy and efficiency of the proposed Algorithm 3.1 for the interface-coupled problem (2.1). The first experiment examines a smooth problem to demonstrate the convergence, while the second applies the algorithm to a three-dimensional model of a steel-titanium composite fuel cell to observe internal heat conduction behavior across the interface. The algorithms are implemented in FreeFEM [16].

5.1. Convergence tests

A smooth problem with an exact solution adapted from [34] is tested using Algorithm 3.1. The problem is set with $T = 1, \Omega_1 = [0,1]\times[0,1], \Omega_2 = [0,1]\times[-1,0], \Gamma = [0,1]\times\{1\}$, $\hat{n}_1 = [0,-1]^\top$ and $\hat{n}_2 = [0,1]^\top$. The exact solution is chosen as follows:

$$\mathbf{u} = \begin{pmatrix} ax(1-x)(1-y)t^3 \\ ax(1-x)\big(c_1 + c_2 y + c_3 y^2\big)t^3 \end{pmatrix},$$

while it also determines the Dirichlet boundary condition, initial condition, and source terms for this smooth problem. The selection of above constants c_1, c_2, c_3 should be determined by (2.1). Inspired by [9], the parameters are chosen as

$$c_1 = 1 + \frac{\nu_1}{\kappa}, \quad c_2 = -\frac{\nu_1}{\nu_2}, \quad c_3 = c_2 - c_1$$

with $a = 1, \nu_1 = 1, \nu_2 = 1, \kappa = 0.1$ for simplicity in this example.

First, consider the convergence with respect to the spatial mesh size h. We apply Algorithm 3.1 to solve problem (2.1) using both linear and quadratic Lagrange Elements with several refined spatial meshes and a fixed time step $\tau = 1/32$. To eliminate the impact of time discretization on the error, a more accurate but slightly more sophisticated approach is introduced as follows. Assuming

$$\mathbf{u}_h^N \approx \mathbf{u}(T,x) + C_1(T,x)\tau^\beta + C_2(T,x)h^\gamma,$$

then it follows that

$$\frac{\left\|\mathbf{u}_h^N - \mathbf{u}_{h/2}^N\right\|_0}{\left\|\mathbf{u}_{h/2}^N - \mathbf{u}_{h/4}^N\right\|_0} \approx 2^\gamma,$$

providing the foundation for calculating the convergence order. Table 5.1 displays the errors, defined as $\|\mathbf{u}_h^N - \mathbf{u}_{h/2}^N\|_0$, along with the convergence orders in space for linear ($r = 1$) and quadratic ($r = 2$) Lagrange elements, which coincide with the theoretical analysis ($r + 1$).

We investigate temporal convergence using both linear and quadratic Lagrange elements with a fixed spatial mesh size $h = 1/32$ and various refined time steps τ. Table 5.2 presents the results, demonstrating that Algorithm 3.1 achieves orders consistent with the theoretical analysis ($2 - \alpha$). Notably, the quadratic Lagrange element yields nearly identical results to the linear Lagrange element, suggesting that low-order finite elements can preserve temporal accuracy while reducing computational costs. The table also illustrates the algorithm's stability and precision, even with large time steps τ.

Table 5.1: Errors and convergence orders with $\tau = 1/32$.

r	h	$\alpha = 0.25$		$\alpha = 0.5$		$\alpha = 0.75$	
		Error	Order	Error	Order	Error	Order
1	1/4	1.04E-01	-	1.02E-01	-	1.00E-01	-
	1/8	2.66E-02	1.97	2.61E-02	1.97	2.55E-02	1.98
	1/16	6.68E-03	1.99	6.54E-03	1.99	6.39E-03	1.99
	1/32	1.67E-03	2.00	1.64E-03	2.00	1.60E-03	2.00
	1/64	4.18E-04	2.00	4.10E-04	2.00	4.00E-04	2.00
	1/128	1.05E-04	2.00	1.02E-04	2.00	1.00E-04	2.00
2	1/4	4.58E-03	-	4.57E-03	-	4.57E-03	-
	1/8	5.71E-04	3.00	5.71E-04	3.00	5.71E-04	3.00
	1/16	7.13E-05	3.00	7.13E-05	3.00	7.14E-05	3.00
	1/32	8.91E-06	3.00	8.91E-06	3.00	8.92E-06	3.00
	1/64	1.11E-06	3.00	1.11E-06	3.00	1.12E-06	3.00
	1/128	1.39E-07	3.00	1.39E-07	3.00	1.39E-07	3.00

5.2. Heat conduction in steel-titanium fuel cell

Composite materials, such as steel-titanium and copper-aluminium plates, are extensively used in fuel cell bipolar plates, offering environmental advantages, low costs, and excellent mechanical properties. Given that temperature critically affects cell performance and lifespan, we focus on thermal management by examining heat conduction within a three-dimensional steel-titanium composite plate fuel cell model [34].

Table 5.2: Errors and convergence orders with $h = 1/32$.

r	τ	$\alpha = 0.25$		$\alpha = 0.5$		$\alpha = 0.75$	
		Error	Order	Error	Order	Error	Order
1	1/4	4.95E-03	-	9.27E-03	-	1.92E-02	-
	1/8	1.56E-03	1.66	3.58E-03	1.37	8.83E-03	1.12
	1/16	4.59E-04	1.76	1.34E-03	1.42	3.91E-03	1.18
	1/32	1.34E-04	1.78	4.93E-04	1.44	1.69E-03	1.21
	1/64	3.93E-05	1.77	1.80E-04	1.46	7.25E-04	1.22
	1/128	1.17E-05	1.75	6.50E-05	1.47	3.08E-04	1.24
2	1/4	4.96E-03	-	9.30E-03	-	1.92E-02	-
	1/8	1.56E-03	1.66	3.59E-03	1.37	8.85E-03	1.12
	1/16	4.60E-04	1.76	1.34E-03	1.42	3.92E-03	1.18
	1/32	1.34E-04	1.78	4.94E-04	1.44	1.70E-03	1.21
	1/64	3.94E-05	1.77	1.80E-04	1.46	7.27E-04	1.22
	1/128	1.17E-05	1.75	6.51E-05	1.47	3.09E-04	1.24

Here, we consider two materials that can be distinctly represented in the conceptual domain as $[0,2]\times[0,4]\times[0,2]\cup[0.5,1.5]\times[1,3]\times[2,3]\cup[0.5,1.5]\times[1,3]\times[3,4]\cup[0,2]\times[0,4]\times[4,6]$ (Fig. 5.1). For simplicity, a Dirichlet boundary condition of $u_1(x,t) = 20$ only is applied to the leftmost edge of the steel plate. Additionally, all other model surfaces, barring the interface, are subject to homogeneous Neumann boundary conditions $\nabla u_i \cdot \hat{n}_i = 0,\ i = 1, 2$. The model starts with an initial condition of 0, and external source terms are excluded. The heat conductivities are set to 60 for steel and 20 for titanium.

Using Algorithm 3.1 with $h = 1/16$ and $\tau = 0.01$, we simulate heat transfer within the steel-titanium composite plate fuel cell model. Fig. 5.2 depicts long-term heat transfer simulations from steel to titanium plates for various derivative orders α. Heat gradually migrates from steel to titanium over time. Rapid heating of the steel plate occurs due to its high thermal conductivity. At the steel-titanium interface, a distinct temperature jump is evident, demonstrating the effect of the interface conditions. The figure demonstrates increased heat transfer to the titanium plate and accelerated diffusion as α rises. This behavior aligns with Caputo fractional derivatives' properties. Higher α values produce results more closely resembling classical diffusion ($\alpha = 1$).

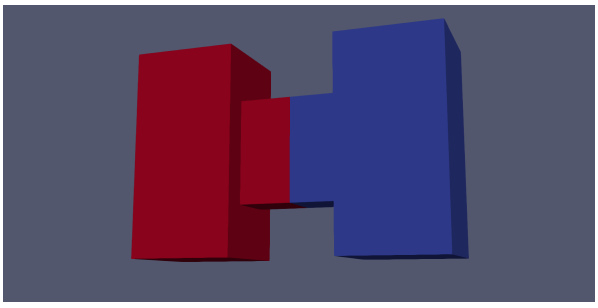

Fig. 5.1. Domain of steel(red)-titanium(blue) composite plate fuel cell model.

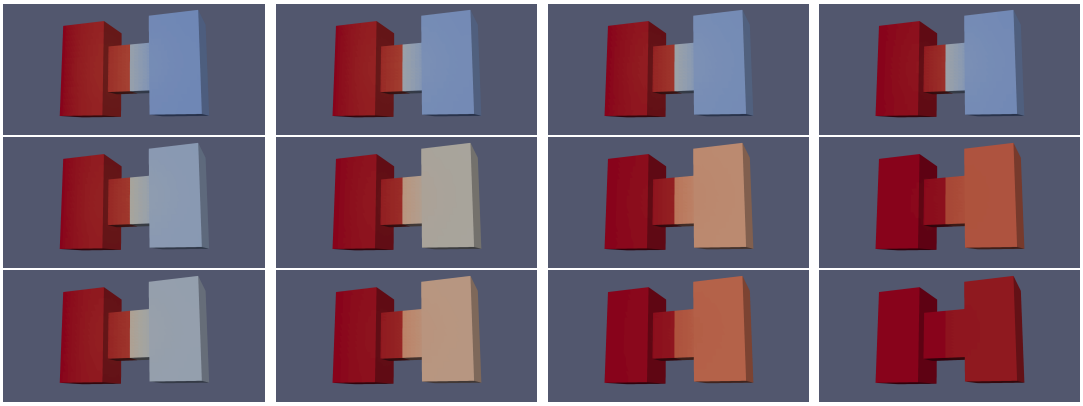

Fig. 5.2. Heat conduction with varying derivative orders α $(0.25, 0.5, 0.75, 1$ from left to right) at different times $(1, 5, 10$ from top to bottom).

6. Conclusions

We introduce a partitioned time-stepping algorithm for an interface-coupled subdiffusion model, utilizing higher-order extrapolation to decouple the problem. This approach allows for information exchange across the interface at each time step, followed by the independent and accurate resolution of individual subproblems. Our theoretical analysis proves the method's unconditional stability and demonstrates optimal order convergence rates in the L^2 norm, which we validate through numerical experiments. This approach can be extended to simulate nonlinear multi-domain models with complex anomalous diffusion behaviors.

Acknowledgements. This work is supported by the National Natural Science Foundation of China (Grant No. 12471406) and by the Science and Technology Commission of Shanghai Municipality (Grant Nos. 22JC1400900, 22DZ2229014) and by the KLATASDS-MOE.

References

[1] D. Bresch and J. Koko, Operator-splitting and Lagrange multiplier domain decomposition methods for numerical simulation of two coupled Navier-Stokes fluids, *Int. J. Appl. Math. Comput. Sci.*, **16**:4 (2006), 419–429.

[2] E. Burman and M.A. Fernández, Stabilized explicit coupling for fluid-structure interaction using Nitsche's method, *C.R. Math.*, **345**:8 (2007), 467–472.

[3] Y. Cao, M. Gunzburger, X. Hu, F. Hua, X. Wang, and W. Zhao, Finite element approximations for Stokes-Darcy flow with Beavers-Joseph interface conditions, *SIAM J. Numer. Anal.*, **47**:6 (2010), 4239–4256.

[4] P. Causin, J.F. Gerbeau, and F. Nobile, Added-mass effect in the design of partitioned algorithms for fluid-structure problems, *Comput. Methods Appl. Mech. Engrg.*, **194**:42 (2005), 4506–4527.

[5] A. Çeşmelioğlu and B. Rivière, Analysis of time-dependent Navier-Stokes flow coupled with Darcy flow, *J. Numer. Math.*, **16**:4 (2008), 249–280.

[6] N. Chen, M. Gunzburger, and X. Wang, Asymptotic analysis of the differences between the Stokes-Darcy system with different interface conditions and the Stokes-Brinkman system, *J. Math. Anal. Appl.*, **368**:2 (2010), 658–676.

[7] J.M. Connors, An ensemble-based conventional turbulence model for fluid-fluid interaction, *Int. J. Numer. Anal. Model.*, **15** (2018), 492–519.

[8] J.M. Connors, J.S. Howell, and W.J. Layton, Partitioned time stepping for a parabolic two domain problem, *SIAM J. Numer. Anal.*, **47**:5 (2009), 3526–3549.

[9] J.M. Connors, J.S. Howell, and W.J. Layton, Decoupled time stepping methods for fluid-fluid interaction, *SIAM J. Numer. Anal.* **50**:3 (2012), 1297–1319.

[10] C. D'Angelo and P. Zunino, Robust numerical approximation of coupled Stokes' and Darcy's flows applied to vascular hemodynamics and biochemical transport, *ESAIM Math. Model. Numer. Anal.*, **45**:3 (2011), 447–476.

[11] K. Diethelm, *The Analysis of Fractional Differential Equations: An Application-Oriented Exposition Using Differential Operators of Caputo Type*, in: *Lecture Notes in Mathematics*, Springer, Vol. 2004, 2010.

[12] M. Discacciati, E. Miglio, and A. Quarteroni, Mathematical and numerical models for coupling surface and groundwater flows, *Appl. Numer. Math.*, **43**:1 (2002), 57–74.

[13] M. Discacciati, A. Quarteroni, and A. Valli, Robin-Robin domain decomposition methods for the Stokes-Darcy coupling, *SIAM J. Numer. Anal.*, **45**:3 (2007), 1246–1268.

[14] M. González-Olvera, L. Torres, J. Hernández-Fontes, and E. Mendoza, Time fractional diffusion equation for shipping water events simulation, *Chaos Solitons Fractals*, **143** (2021), 110538.

[15] D. Han, X. Wang, and H. Wu, Existence and uniqueness of global weak solutions to a Cahn-Hilliard-Stokes-Darcy system for two phase incompressible flows in karstic geometry, *J. Differential Equations*, **257**:10 (2014), 3887–3933.

[16] F. Hecht, New development in FreeFem++, *J. Numer. Math.*, **20**:3–4 (2012), 251–266.

[17] J. Hou, M. Qiu, X. He, C. Guo, M. Wei, and B. Bai, A dual-porosity-Stokes model and finite element method for coupling dual-porosity flow and free flow, *SIAM J. Sci. Comput.*, **38**:5 (2016), B710–B739.

[18] K. Lätt and A. Pedas, Numerical schemes for a class of singular fractional integro-differential equations, *Appl. Numer. Math.*, **200** (2024), 331–343.

[19] W.J. Layton, F. Schieweck, and I. Yotov, Coupling fluid flow with porous media flow, *SIAM J. Numer. Anal.*, **40**:6 (2002), 2195–2218.

[20] W. Layton, H. Tran, and X. Xiong, Long time stability of four methods for splitting the evolutionary Stokes-Darcy problem into Stokes and Darcy subproblems, *J. Comput. Appl. Math.*, **236**:13 (2012), 3198–3217.

[21] C. Li and Q. Yi, Finite difference method for two-dimensional nonlinear time-fractional subdiffusion equation, *Fract. Calc. Appl. Anal.*, **21**:4 (2018), 1046–1072.

[22] D. Li, H.-L. Liao, W. Sun, J. Wang, and J. Zhang, Analysis of $L1$-Galerkin FEMs for time-fractional nonlinear parabolic problems, *Commun. Comput. Phys.*, **24**:1 (2018), 86–103.

[23] Z. Li, H. Wang, and D. Yang, A space-time fractional phase-field model with tunable sharpness and decay behavior and its efficient numerical simulation, *J. Comput. Phys.*, **347** (2017), 20–38.

[24] Y. Lin and C. Xu, Finite difference/spectral approximations for the time-fractional diffusion equation, *J. Comput. Phys.*, **225**:2 (2007), 1533–1552.

[25] J.-L. Lions, R. Temam, and S. Wang, Models for the coupled atmosphere and ocean, *Comput. Mech. Adv.*, **1**:1 (1993), 3–4.

[26] F. Liu, S. Shen, V. Anh, and I. Turner, Analysis of a discrete non-Markovian random walk approximation for the time fractional diffusion equation, *ANZIAM J.*, **46** (2005), 488–504.

[27] Z. Luo, X. Zhang, S. Wang, and L. Yao, Numerical approximation of time fractional partial integro-differential equation based on compact finite difference scheme, *Chaos Solitons Fractals*, **161** (2022), 112395.

[28] C. Lv and C. Xu, Error analysis of a high order method for time-fractional diffusion equations, *SIAM J. Sci. Comput.*, **38**:5 (2016), A2699–A2724.

[29] M. Mu and X. Zhu, Decoupled schemes for a non-stationary mixed Stokes-Darcy model, *Math. Comp.*, **79**:270 (2009), 707–731.

[30] Z. Odibat and D. Baleanu, Numerical simulation of nonlinear fractional delay differential equations

with Mittag-Leffler kernels, *Appl. Numer. Math.*, **201** (2024), 550–560.

[31] X. Qi and C. Xu, An efficient numerical method to the stochastic fractional heat equation with random coefficients and fractionally integrated multiplicative noise, *Fract. Calc. Appl. Anal.*, **27**:5 (2024), 2754–2780.

[32] A. Quarteroni, A. Veneziani, and P. Zunino, Mathematical and numerical modeling of solute dynamics in blood flow and arterial walls, *SIAM J. Numer. Anal.*, **39**:5 (2002), 1488–1511.

[33] L. Shan and H. Zheng, Partitioned time stepping method for fully evolutionary Stokes-Darcy flow with Beavers-Joseph interface conditions, *SIAM J. Numer. Anal.*, **51**:2 (2013), 813–839.

[34] Y. Sun, J. Wang, and H. Zheng, Novel partitioned time-stepping algorithms for fast computation of random interface-coupled problems with uncertain parameters, *Numer. Math. Theory Methods Appl.*, **17**:1 (2024), 145–180.

[35] Z.-Z. Sun and X. Wu, A fully discrete difference scheme for a diffusion-wave system, *Appl. Numer. Math.*, **56**:2 (2006), 193–209.

[36] H. Wang and X. Zheng, A modified time-fractional diffusion equation and its finite difference method: Regularity and error analysis, *Fract. Calc. Appl. Anal.*, **22**:4 (2019), 1014–1038.

[37] S.B. Yuste and L. Acedo, An explicit finite difference method and a new von Neumann-type stability analysis for fractional diffusion equations, *SIAM J. Numer. Anal.*, **42**:5 (2005), 1862–1874.

[38] F. Zeng, C. Li, F. Liu, and I. Turner, The use of finite difference/element approaches for solving the time-fractional subdiffusion equation, *SIAM J. Sci. Comput.*, **35**:6 (2013), A2976–A3000.

[39] H. Zhang, X. Jiang, and F. Liu, Error analysis of nonlinear time fractional mobile/immobile advection-diffusion equation with weakly singular solutions, *Fract. Calc. Appl. Anal.*, **24**:1 (2021), 202–224.

[40] X. Zheng and H. Wang, Optimal-order error estimates of finite element approximations to variable-order time-fractional diffusion equations without regularity assumptions of the true solutions, *IMA J. Numer. Anal.*, **41**:2 (2021), 1522–1545.